World Journal of Environmental Biosciences
Available Online at: **www.environmentaljournals.org**

Volume 14, Issue 4: 71-81

https://doi.org/10.51847/qrULNAz8q6

ISSN 2277- 8047

Overview of the Features of Specialised Maritime Transport for the Transport of Green Hydrogen

Syrlybekkyzy Samal[1], Nurmaganbet Ermek[2], Serikbayeva Akmaral[1], Amankeshuly Dastan[1], Jumasheva Kamshat[1]*, Ramazan Akhmet[1], Dedova Tatyana[3], Iskakov Berik[3], Merekeev Aibek[3]

[1]Department of Ecology and Life Safety, Yessenov University, Aktau, Kazakhstan.
[2]Department of Jurisprudence, Yessenov University, Aktau, Kazakhstan.
[3]LLP "Ionosphere Institute", Almaty, Kazakhstan.

ABSTRACT

The approach for a thorough evaluation of the structural soundness of type C tanks meant for the storage and transportation of liquid hydrogen is proposed in this work. An assessment process for cargo compartments for liquid hydrogen employing Type C tanks in accordance with MMO specifications is described, and the design assessment procedures used for ships transporting cryogenic cargo are examined. Thermal analysis, structural and fatigue assessments, and, if required, fracture propagation analysis are all part of this process. The established methodology's ability to verify structural integrity was evaluated. The idea and design of specialized tanks for the storage and transportation of green hydrogen on ships destined for use in the Caspian Sea were developed. The main emphasis is on creating cryogenic containers with highly efficient vacuum insulation, which minimizes hydrogen losses by reducing evaporation during transportation. The project envisages the use of materials resistant to extremely low temperatures and mechanical stress, as well as the introduction of thermoregulation systems to maintain stable storage conditions. Particular attention was paid to compliance with international standards, including IMO and IGC Code requirements, which ensures high safety of tank operation.

Keywords: *Hydrogen, Liquefied gas, Reservoir, Material properties, Analysis*

Corresponding author: Jumasheva Kamshat
e-mail ✉ kamshat.jumasheva@yu.edu.kz
Received: 02 September 2025
Accepted: 23 November 2025

INTRODUCTION

In order to combat global warming and replace fossil fuels, the switch to a range of alternative energy sources is quickening globally. Nowadays, liquefied natural gas is being considered as a means of achieving goals for lowering emissions of sulfur and nitrogen oxide (Mingzheng *et al*., 2025).

In addition, the transition to decarbonization requires hydrogen (H_2) energy, which does not emit carbon dioxide and could become a future natural resource. However, to introduce a hydrogen economy within the country, methods of storing and transporting hydrogen from foreign places of its production are needed (Nasiru *et al*., 2023).

At normal temperature and atmospheric pressure, liquid hydrogen has a volume of about 1/845 that of hydrogen gas; at 700 bar, it is around half that of hydrogen. Because of this, it is the best format for big-scale accumulation and the best way to store large amounts (Ahmad *et al*., 2024).

International maritime shipping accounts for more than 80% of global trade and is responsible for approximately 2.89% of global greenhouse gas (GHG) emissions. The IMO's GHG reduction strategy, revised in 2023 (MEPC 80), sets a target of net-zero emissions by 2050, with an interim target of 5% carbon-free or "near-zero" fuels by 2030. Under the European Green Deal and the REPowerEU plan (European Commission, 2022), green hydrogen is identified as a strategic energy carrier to replace fossil fuels in hard-to-electrify sectors such as aviation, heavy industry and deep-sea shipping.

Liquid hydrogen (LH_2) has the highest mass energy density of any practical fuel — 120 MJ/kg — and emits only water vapour when burned. However, the need to store it at −253 °C (20 K) imposes extremely stringent requirements on tank design, thermal insulation, materials and safety regulations, exceeding anything faced by the LNG industry (Ustolin *et al*., 2022).

The general guidelines for liquid cargo tanks are followed by type A tanks. Complete secondary protection is necessary for major spills if there is a chance that liquid cargo will leak.

This type of tank is commonly used on ships to transport liquefied petroleum gas (LPG).

The structural analysis of Type B tanks is required to verify the structure's safety. By using fatigue crack propagation analysis based on fracture mechanics, assuming crack start, the volume of potential leaks is determined. For this kind of tank, partial secondary barriers are needed.

The purpose of type C tanks is pressure vessels. They eliminate the need for a secondary barrier by guaranteeing the structure's safety and integrity without the possibility of leakage.

Type C tanks are typically spherical or cylindrical pressure vessels with a design pressure higher than two bar. They are

designed and manufactured in accordance with accepted codes or standards for pressure receptacles, such as the ASME Code for Boilers and Pressure Vessels, and are further augmented by the specifications of classification societies and laws.

Transport, storage containers, fire hazards, roll effects, and double-walled vacuum pipes are the primary topics of research on liquid hydrogen tanks. Based on the International Code for the Construction and Equipment of Ships Carrying Liquefied Gases in Bulk (IGC Code), the authors (Choe *et al*., 2016; IMO, 2016; Ahn *et al*., 2017) suggested a structural integrity evaluation process for Type B LNG fuel tanks. To evaluate structural safety, they conducted finite element analysis under various loads.

Divinycell's cryogenic compressive strength, which is utilized in LNG insulation systems, was experimentally assessed in Work (Kim *et al*., 2021). In the study, (Noh *et al*., 2017) conducted a numerical analysis of the technique for evaluating how the insulating system of LNG tankers reacts to shock loads from tilting while accounting for the impact of the hull structure's elastic support. Cryogenic material R-PUF, which is utilized in LNG tanker cargo storage systems, has recently been the subject of experimental research (Song *et al*., 2022).

For membrane-type cargo storage systems subjected to wave action, work (Afif *et al*., 2016) established fracture strength requirements. The strength of these systems was evaluated using the finite element method, and the findings were compared with DNV standards. Studies examining the design assessment of type C tanks for the storage of liquid hydrogen are, nevertheless, incredibly uncommon. An approach is presented in work (Jeerh *et al*., 2021) for calculating the evaporation rate (ER) in type C tanks at various filling levels. Finite element analysis was used to calculate evaporation rates, and the outcomes were contrasted with experimental data. The impact of waves on heat transmission and the quantity of evaporated gas production was numerically analyzed in work (VTT, 2019). Work (Daniel *et al*., 2022) used commercial software and common design codes to assess an independent Type C tank's design thickness. Although a (IGC CODE, 1986) materials-based optimization was carried out for the design and use of liquefied hydrogen type C tanks, it did not offer a comprehensive process for the tank design itself.

The IMO Gas Carrier Code (IGC Code, 2016; updated MSC.565(108), 2024) classifies independent cargo tanks into Types A, B and C, as well as membrane structures.

Type C tanks are the standard for liquid hydrogen, as their pressure vessel design (P_0 > 2.0 bar) eliminates the need for a second barrier while ensuring structural integrity. (Kim *et al*., 2024) developed a structural integrity assessment methodology for a conceptual design of a liquid hydrogen carrier with a capacity of 23,000 m^3, including seven design loading cases according to the IGC Code: hydrostatic loads, dynamic accelerations in three directions, cargo vapour pressure, external shell vacuum, and thermal stresses during filling/emptying. The maximum equivalent stress according to Mises was 272 MPa (localised, permissible according to the IGC Code), and the stability margin coefficient of the external vacuum shell was 2.9 at a vacuum pressure of 0.1 MPa.

Cylindrical and spherical Type C tanks are mounted on saddle supports — one fixed, one sliding to compensate for axial thermal expansion (ΔL ≈ 36 mm per 18 m at ΔT = 276 K). The supports are made of G-10CR fibreglass gaskets with low thermal conductivity (λ ≈ 0.29 W/(m·K)), which provide mechanical strength with minimal heat transfer from the warm outer shell to the cold inner tank (Ustolin *et al*., 2022; Kim *et al*., 2024).

Development of a structural evaluation procedure for liquid hydrogen tanks

Because of design elements that strengthen its structure and do away with the requirement for a secondary barrier, Type C tanks are regarded as airtight. Because of their benefits, they are frequently utilized as LNG fuel tanks on ships and are appropriate for light-duty LNG, ammonia, or LPG carriers (Liquefied Gas Handling Principles On Ships and in Terminals, 2000).

Two kinds of support structures are employed for spherical or cylindrical tanks: sliding and fixed. The independent tank is firmly secured by fixed supports, yet it can expand and compress as necessary thanks to sliding supports (Wang *et al*., 2015).

As seen in picture 1, tanks can have one or two walls. In single-layer tanks, insulating gaskets are positioned between the support seat and the tank structure, and the exterior is coated with insulating material. Vacuum insulation is put in two-layer tanks, and plastic supports or insulating materials are placed in between the inner and outer layers. When it comes to pressure retention, two-layer tanks have an advantage over single-layer tanks (Rötzer *et al*., 2020).

Procedure for assessing structural strength. A full process for determining a Type C tank's strength for liquid hydrogen is depicted in picture 2. Heat transfer analysis and evaporation rate computation, structural analysis, loss of stability analysis, and fatigue and fracture propagation analysis are the several steps that make up the tank integrity testing methodology (Alikin., 2005).

Because liquid hydrogen has a temperature of -253°C, heat transfer analysis is an essential part of the design process for a C-type tank. Choosing the steel grade for the hull and calculating heat loads for structural strength analysis are the two primary goals of this analysis. Heat transfer analysis is also used to determine the evaporation rate. The ambient temperature parameters in this instance are different from those that are utilized to determine the steel grade. While the evaporation rate is computed under the IMO's warm temperature settings, the choice of steel is subject to the thermal design conditions established by the IMO. Complex thermostructural analyses to examine the thermal connections between the tank shell, the wooden insulation, and the support structures are necessary to evaluate the strength of a Type C tank for liquid hydrogen (Kim *et al*., 2024).

Thermal and mechanical loads were used in a sequential conjugate thermal structural computation (Green *et al*., 2023; Guillen *et al*., 2023; Lembo *et al*., 2023; Johansson *et al*., 2024; Kristensen & Pedersen, 2024; Kulkarni *et al*., 2024; Bianchi *et al*., 2025; Mikhailov & Sorokina, 2025). Steam and liquid pressure are included in the design internal pressure. Without accounting for the stresses from waves, the combined effects of acceleration and gravity result in liquid pressure. Each tank component was calculated in the structural study under static conditions, at 30° roll, under collision conditions, and under normal running conditions with maximum acceleration.

It was determined using the IGC algorithm how resistant the

tank was to losing stability under external pressure. The eigenvalue approach in finite element analysis is used to find the value of the design external pressure and compute the critical collapse pressure. Fracture mechanics and crack propagation considerations are added to the pressure vessel criteria, which serve as the foundation for the design of an independent Type C tank. The fatigue strength of the complete tank structure was assessed. Low-cycle fatigue brought on by thermal loads from the load and high-cycle fatigue resulting from recurrent loads during the service life were evaluated in the fatigue study.

The repeated history of loads during the service life is the primary cause of high-cycle fatigue, with wave loads having a substantial impact on both independent self-supporting tanks and conventional ships. Fatigue damage is intimately correlated with the distribution of stress caused by long-term wave action. In order to account for real-world environmental circumstances, direct load analysis and stochastic analysis are typically used to evaluate the long-term stress distribution during the design phase (Ejikeugwu *et al*., 2023; Joshi *et al*., 2023; Mansour *et al*., 2023; Dupont & Lefevre, 2024; Evans *et al*., 2024; Fischer *et al*., 2024; Yılmazer & Altinok, 2024; Chen *et al*., 2025; Herrera *et al*., 2025; Morales *et al*., 2025). In order to streamline the process, this study utilizes simplified load histories based on the Weibull distribution, which is a technique from international rules (IGC Code; IMO, 1986).

Additionally, because of temperature changes during loading and unloading, hydrogen cargo tanks undergo thermal stresses both inside and outside. It is important to evaluate low-frequency fatigue in addition to high-frequency fatigue since stress ranges might be extremely high even with a small number of cycles (Zhou *et al*., 2014).

For regions subjected to high stresses under recurring static loads, low-frequency fatigue is typically taken into account. An analysis based on fracture mechanics is required for crucial places in the tank design with significant dynamic stresses. According to the fracture mechanics approach, the idealized crack spreads according to the range of the stress intensity component (Tomioka *et al*., 2011).

To verify the integrity of the construction, an analysis of fatigue fracture propagation for the tank skin and internal structure was carried out. Crack propagation was evaluated from the first crack to the critical size. For the investigation of crack propagation, regions with large concentrations of stress or substantial fatigue damage were chosen.

Based on the results of parametric optimisation (Naquash *et al*., 2024) determined that 40-layer MLI with silk mesh spacers provides a heat flux of 1.01 W/m^2 and an evaporation rate of 0.01–0.05%/day for a 500-litre tank. (Yin *et al*., 2024) confirmed in their review of insulation technologies that glass bubbles combined with MLI are preferable to perlite: their apparent thermal conductivity at high vacuum is 15–22% lower, and their bulk density is lower, which reduces the load on the structure. Multi-layer insulation (MLI) — a set of reflective screens made of aluminium foil or metallised Mylar alternating with silk mesh or fibreglass spacers under deep vacuum (< 10^{-4} mbar) — recognised as the most effective passive thermal insulation for cryogenic liquid fuel tanks.

Combining sprayed polyurethane foam insulation (SOFI) as a backing layer with MLI in a vacuum space reduces assembly pressure and increases the vibration resistance of the structure. Vapour-cooled screens (VCS) use the heat capacity of the outgoing cold hydrogen vapour stream to intercept heat flow at an intermediate temperature level, reducing the total heat influx. (Liu *et al*., 2023) showed that increasing the diameter of VCS pipes reduces heat flux by 32%, and doubling the number of pipes reduces it by 49%.

(Ghaffari-Tabrizi *et al*., 2022) from the German Aerospace Centre (DLR, Austria), using the EcoSimPro/ESPSS platform, found that pre-cooling the receiving tank with liquid nitrogen before refuelling reduces evaporation losses during bunkering by approximately 30%. This result has direct implications for the design of liquid hydrogen bunkering facilities in European and Caspian ports.

Numerical model of a marine vessel for transporting liquefied hydrogen

The vessel under study is a marine tanker for the transport of liquefied hydrogen. Here, x is the longitudinal distance between the center of the vessel and the tank's center of gravity (CG), y is the lateral distance between the centerline and the tank's center of gravity, and z is the vertical distance between the actual waterline and the tank's DH. In most cases, coefficient K is assumed to be 1.

For specific loading conditions and enclosure shapes, the value of K defined as K=13GMB/B, where GM - metacentric height, a B - width of the vessel.

The inner and outer tanks, as well as the inner supports (which are composed of GRE G-10 material) and the exterior supports, are the primary parts of the tank that is being studied, as illustrated in **Figure 1**. The fiberglass-epoxy composite material GRE G-10—is widely utilized in many different industries because of its special qualities, which include high strength, chemical resistance, and strong electrical performance. Glass Reinforced Epoxy, or "glass fiber reinforced epoxy composite," is what GRE stands for. Due to its exposure to extremely low temperatures and high internal pressures, the inner tank is the most crucial component.

The outer tank has vacuum insulation filled with glass bubble material and is made to safely enclose and shield the inner citstern. The support that connects the inner and exterior tanks is composed of epoxy resin strengthened with glass. The exterior tank and saddles are joined by welding, and the entire tank structure is supported by two saddle supports. The tank's length is 31,500 mm, while the cylindrical portion's diameter is roughly 18,000 mm. The vessel's four liquid hydrogen storage tanks, each with a 5,750 m^3 capacity, are its primary features.

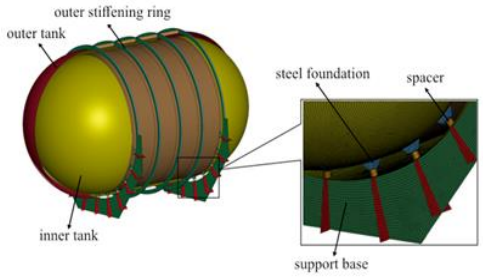

Figure 1. Finite element model of the target cargo tank (Tomioka *et al*., 2011).

A global finite element model was created using four-node shell

elements for tank and saddle structures, eight-node volumetric elements for a GRE spacer, and contact elements for interactions between the tank, GRE spacer and saddle supports. The shell elements' dimensions of 100 mm by 100 mm guarantee convergence to the rated voltage determined by applying the formula for the circumferential tension in a cylindrical shell. External and internal tanks made of SUS304L stainless steel. The spacers are composed of GRE G-10 material, while the saddles are made of mild steel.

Because it is subjected to extremely low cryogenic temperatures and tremendous internal pressure, the internal tank is the most crucial component of the tank in issue. An exterior tank was created to encircle the internal container for its secure preservation. Glass microspheres are placed into the vacuum-insulated exterior tank. Glass fiber-reinforced epoxy composite supports were used to connect the inner and exterior tanks. The exterior tank and saddle were welded together, and the entire tank construction was supported by two saddle supports.

As recommended by the International Maritime Organization, the ambient temperature for the heat transfer analysis was set at 5°C. The temperature of liquid hydrogen was −253°C, and the heat transfer coefficient under natural convection was estimated to be 5 W/m^2 K. The thermal boundary conditions are depicted in full in **Figure 2a**. As shown in **Figure 2**, all degrees of freedom in the underside assembly of the saddle supports fastened to the vessel's hull were fixed. B. By defining the coefficient of friction between the spacer and the tanks, the contact conditions were also considered in order to assess the impact of contact and potential sliding between them.

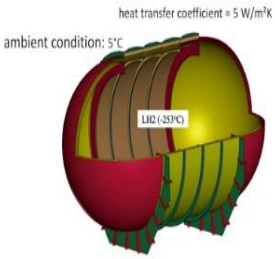

a)

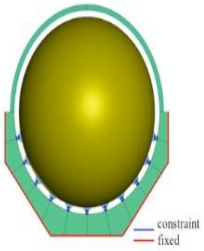

b)

Figure 2. Boundary conditions for the CE target mode. a) Thermal boundary b) Structural boundary

Determining design loads is necessary when designing a type C liquid hydrogen tank. The density of the materials employed and the acceleration of gravity are taken into consideration when calculating the tank's dead weight as an inertial load. The inside tank experiences an internal load from the vacuum insulation system's low-temperature vacuum pressure, while the outer shell experiences an external load. Assuming that the ambient temperature is -5°C and the design temperature of liquid hydrogen is -253°C, thermal loads were acquired from steady-state heat transfer calculations to compute the temperature distribution over the entire tank and its support structures. To evaluate the impact of mechanical and thermal loads on the tank's integrity, the temperature distribution findings from the thermal analysis were incorporated into a structural analysis model. For the design of type C tanks, the IGC Code makes use of conventional pressure vessel calculation methods, fracture mechanics, and crack propagation criteria. The following formulas are used to calculate the minimum design vapor pressure.

$$P_0 = 0.2 + AC(\rho_r)^{1.5}\ (MPa) \tag{1}$$

$$A = 0.00185(\frac{\sigma_m}{\Delta\sigma_A}) \tag{2}$$

The acceptable dynamic membrane stress ΔσA is 25 MPa for aluminum alloys and 55 MPa for ferrite-pearlite, martensitic, and austenitic steels. The hydrostatic pressure from partially full fresh water plus 1.5 times the steam pressure constitute the tank test conditions. The longitudinal acceleration in an emergency accident simulation is set to half the acceleration of gravity (9.81 m/s^2).

There are various methods to ascertain dynamic loads, including using accelerometers on a full-scale vessel to measure accelerations, doing a seaworthiness investigation, or testing models. The acceleration components in this study are computed using the IGC Code recommendations, which correspond to a probability level of 10^{-8} for the conditions pertaining to the Eurasia and Central Asia basins.

$$a\_z = \pm a\_0\ \sqrt{(1 + \ 〚(5.3 - 45/L)〛\ \hat{}\ 2\ \ 〚(x/L + 0.05)〛\ \hat{}\ 2\ \ 〚(0.6/C\_\text{B}\ )〛\ \hat{}\ 2 + \ 〚((0.6yK\hat{}\ 1.5)/B)〛\ \hat{}\ 2\ )} \tag{3}$$

$$a\_y = \pm a\_0\ \sqrt{(0.6 + 2.5(x/L + 0.05)\hat{}\ 2 + K(1 + 0.6K\ z/B\ )\hat{}\ 2\ )} \tag{4}$$

$$a_x = \pm a_0\sqrt{0.6 + A^2 - 0.25A} \tag{5}$$

$$a_0 = 0.2\frac{V}{\sqrt{L}} + \frac{34 - (\frac{600}{L})}{L} \tag{6}$$

$$A = (0.7 - \frac{L}{1200} + 5\frac{z}{L})(\frac{0.6}{C_B}) \tag{7}$$

The highest dimensionless accelerations (in relation to the acceleration of gravity) in the respective directions are indicated by the ax, ay, and az. Static weight is not taken into

consideration by the az component; ax contains static weight longitudinally owing to trim, and ay includes static weight transversely due to roll.

Calculated load cases. It is necessary to ascertain all design loads while creating a type C tank for liquid hydrogen. Tank tare weight is regarded as an inertial load, accounting for both the density of the materials and the acceleration of gravity. The internal reservoir is internally loaded by the insulation system's low temperature vacuum pressure. Every load scenario listed in the IGC Code is considered when evaluating a tank's structural integrity.

Acceptance criteria. A pressure vessel is a separate kind C tank used to transport liquid hydrogen. In compliance with the IGC Code and other globally recognized requirements for pressure receptacles, the structural stress analysis findings were assessed to ascertain the yield strength. The computed stresses should not be more than the corresponding allowable values listed in **Table 1** for designing such tanks.

Table 1. Permissible voltage value for type C tanks for liquid hydrogen (Liquefied Gas Handling Principles On Ships and in Terminals, 2000)

Voltage designation	Acceptable voltage value
σm	≤f
σL	≤1.5f
σb	≤1.5f
σL+σb	≤1.5f
σm+σb	≤1.5f
σm+σb+σg	≤3.0f
σL+σb+σg	≤3.0f

Here, f stands for the computed allowable voltage, which is computed as f = min (Rm/A, Re/B), where Re is the minimum yield strength at room temperature. If there is no discernible yield strength in the "stress-strain" curve, a conditional yield strength of 0.2% strain is used. The minimum room temperature temporal resistance, or Rm parameter, is shown in **Tables 2 and 3**.

Table 2. Values A and B for calculating the permissible voltage

Parameter	Nickel steels and carbon-manganese steels	Austenitic steel	Aluminum alloy
A	3.0	3.5	4.0
B	1.5	1.5	1.5

Table 3. Acceptable stresses of the material

Material	Re (MPa)	Rm (MPa)	F (MPa)	1.5f (MPa)	3.0f (MPa)	0.9Re (MPa)
SUS304	175.0	480.0	116.7	175.0	350.0	157.5
Carbon steel	235.0	400.0	114.3	171.0	343.0	211.5

Theromostructural modeling of the design of a tank for liquid hydrogen

Heat transfer analysis. Two phases of thermostructural study were completed. The temperatures of the structural elements were ascertained at the first step by heat transfer modeling, and at the second stage, structural analysis was conducted while accounting for all other mechanical loads and the thermal loads discovered at the first stage. The findings of a heat exchange analysis for a liquid hydrogen tank (LH_2) are shown in **Figure 3**. A minimum temperature of -253°C was noted on the internal reservoir that is in direct contact with LH2, while a maximum temperature of 3.3°C was noted on the saddle support. Because steel has a strong thermal conductivity, the steel base connected to the inner tank attained the same temperature as liquid hydrogen. Due to the vacuum insulation provided by glass bubbles in the annular area between the inner and outer tanks, the structure surrounding the inner tank experienced very little change in temperature. However, as **Figure 3** illustrates, the struts, which are composed of GRE G-10 material with extremely poor thermal conductivity, were exposed to the largest shift in the thermal gradient.

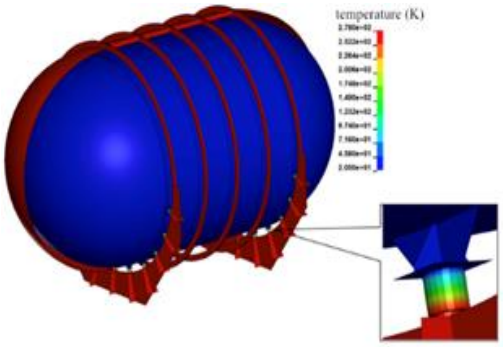

Figure 3. Summary of the heat transfer analysis's findings

structural evaluation. The LS-DYNA program was used for the structural study in order to assess the tanks' displacement and the stresses produced under various loads

The total of the most important stresses—local, bending, and secondary stresses—as well as the associated allowable values are provided. Even for LC7, the optimal hydrostatic test circumstances, the final stress is not above 90% of the allowable value specified in the IGC Code, and all stress components satisfy the requirements. The cargo tank's existing design and its supports meet the IGC Code's yield strength standards.

Von Mises equivalent voltages were computed for each of the seven load scenarios that were examined. A flow test was carried out for every part, including the two saddle supports and the inner and outer reservoirs. Emergency collision scenarios, which are thought to be the most loaded of all, were used to create stress contours. The loads operating on the interior tank are most affected by the internal pressure, which comprises steam pressure, cargo pressure, and cold vacuum pressure. For instance, the internal tank's primary membrane voltage of 112 MPa is less than the allowed limit of 116.7 MPa. Stresses have developed at the intersection of the inner tank and the steel support as a result of the inner tank compressing due to a high temperature gradient. The region where the steel support is fastened to the interior tank exhibits a maximum stress of 272 MPa. Because it is assessed in a crucial location and is brought on by the combined effects of thermal and other mechanical loads, this stress is categorized as localized.

Description of the stability loss of tanks

When subjected to external pressures and other stressors that result in compressive stresses, cylindrical shells and

torospheric or ellipsoidal bottoms are typically susceptible to the requirements for loss of stability analysis. With finite element eigenvalue (FEM) analysis, many buckling modes can be identified. Furthermore, two FEM techniques can be used to establish the critical tank loss pressure: a post-critical stability study with an imposed initial error and a linear loss analysis (eigenvalue analysis).

In order to determine the eigenvalues corresponding to loss of stability modes, linear loss of stability analysis (also known as eigenvalue analysis) necessitates the use of a unit distributed load and the elastic properties of the tank material. In general, a crucial buck load is represented by the first buck mode with the lowest eigenvalue.

However, in order to account for notable variations in the tank geometry, a post-critical stability analysis should be carried out. This will necessitate both the material's elastic-plastic qualities and a distributed load applied to the tank while accounting for the current variations. Real measurements, manufacturing tolerances, or stability loss forms derived from eigenvalue analysis can all be used to calculate the deviation field.

In this investigation, linear stability loss analysis was used to assess the exterior tank's stability loss strength at a vacuum pressure of 0.1 MPa. The FEM results indicated a safety factor of 2.9 and a critical buckling pressure of 0.29 MPa, which are in line with the IGC Code's specifications.

Calculation of the evaporation rate of liquid hydrogen from tanks

The rate of evaporation and loss of liquefied gases, such as LNG or liquefied hydrogen (LH_2), from tanks or cargo compartments is reflected by evaporation, which is a common technique in the transportation of liquefied gases. The amount of gas that evaporates in a specific amount of time is known as speed isarenia, and it is often represented as a percentage per day. This parameter has a major impact on the economic viability and efficiency of gas management when it comes to the design and operation of ships or storage facilities (Demir & Kaya, 2023; Joshi *et al*., 2023; Pinto & Sousa, 2023; Wilson *et al*., 2023; Adams *et al*., 2024; Csep *et al*., 2024; Karimov & Rakhimova, 2024; Morozov *et al*., 2025; Chen *et al*., 2025; Romero & Campos, 2025). Evaporated gas is created when liquefied gases evaporate at temperatures higher than the boiling point. Heat gain is the primary cause of evaporating gas generation on ships, although there are other contributing factors as well. Since heat inflow into cargo tanks is the only source of evaporating gas production, the evaporation rate in this study was determined.

The following formula can be used to get the evaporation rate, which is the proportion of liquid hydrogen that evaporates daily in relation to the original amount of liquid hydrogen loaded.

$$BOR = \frac{\sum Q_{leak}}{\rho_{LH2 \times V_{liq} \times \lambda}} \times 3600 \times 24 \times 100\% \quad (8)$$

$$Q_{leak} = UA\Delta T \quad (9)$$

FEM was used to determine the heat loss to the cargo tank by a local steady-state heat transfer analysis. The air and seawater temperatures were assumed to be 45°C and 32°C, respectively, to create a warm atmosphere in accordance with IMO requirements. To move heat from the surroundings to the external reservoir, a convection heat transfer coefficient of 5 W/m^2K was used. Solid-state components were used to mimic a vacuum insulation system with a thermal conductivity of 0.0018 W/m K and fiberglass spacer elements (GRE) with a thermal conductivity of 0.29 W/m K.

The particular requirements for evaporation rates vary depending on the kind of cargo transported, the mode of transportation, the storage facility's layout, and the vessel type. For instance, the evaporation rate for ships transporting LNG is typically computed every day and might vary in percentage every day based on the ship's operation and construction. There are currently no generally recognized norms for evaporation rates for other kinds of cargo, such as liquid hydrogen, and related regulations and standards are in development. Since liquid hydrogen evaporation has a major impact on transportation efficiency, the evaporation rate is very crucial. Therefore, one of the main challenges in designing ships and storage facilities for the transportation of liquid hydrogen is minimizing the rate of evaporation.

The heat flux determined for the inner tank and the distance elements can be extended over the whole region to determine the total heat flux. Eq .8 can be used to calculate a given tank's evaporation rates. This study's method for calculating evaporation rate is an example, and the projected figure for a genuine type C tank might be greater. Although additional heat inflows through the liquid dome, pipe inlets, and hatches may occur under actual operating conditions, this analysis only took into account heat loss through insulation and spacer elements from GRE. Consequently, more precise calculations that account for all potential sources of heat flow into the liquid hydrogen tank are required for the actual design.

Digital modelling (Kavin *et al*., 2025) showed that BOG production from a cylindrical liquid hydrogen tank with a volume of 5.6 m^3 varies by up to 28% depending on seasonal environmental conditions. For routes through the Caspian Basin, where air temperatures range from −10 °C in winter to +45 °C in summer, this makes active thermal management systems a mandatory element of any regional liquid hydrogen carrier's project.

The BoilFAST software tool (Petitpas, 2022), verified using test data from a 125 m^3 liquid hydrogen tank at the NASA Kennedy Space Centre test site, allows self-superheating and cargo losses to be calculated for tanks of arbitrary shape using NIST equations of state. The simulation results show that for a 20,000 m^3 shipboard liquid hydrogen tank with 80-layer MLI, zero evaporation can be achieved by using an integrated refrigeration and storage (IRAS) system based on the Brighton cycle. The integration of a recondensation unit can reduce daily cargo loss by at least 38.7% (Ustolin *et al*., 2022).

Simulation of crack propagation along the walls of liquid hydrogen tanks

In regions where fracture identification is challenging or where there are structural flaws, the integrity of the structure can be evaluated by examining the propagation of cracks. This technique, sometimes referred to as "fracture mechanics analysis" or "Critical Engineering Assessment (CEA)," is used to evaluate an object's durability and structural integrity. This method is mostly applied to nuclear reactors and airplanes, and cryogenic cargo tank design also takes damage resistance and leakage-to-fracture theory into account. The KIO considers the

strength and viscosity of the material, internal and external loads, the length and depth of the fracture, residual stresses from welding, and the assumption that there is a crack in the weld zone. Additionally, the fractured joint is assessed using a fracture assessment diagram (FAD) that considers the features of both load and viscosity. The crack opening parameter (COP) is commonly employed for viscosity assessment.

This study may be used to estimate the long-term voltage that corresponds to the vessel's service life (i.e., probability level (108)). Eq. 10 was utilized to compute the simplified long-term stress distribution using the modified Weibull distribution.

$$log_{10}\, N_i = 8 \times (1.0 \times \frac{\Delta\sigma_i}{\Delta\sigma_0}) \quad (10)$$

To remove the impact of the stress sequence on the fracture propagation lifespan, the entire stress spectrum was split up into 20 groups. It was believed that the fatigue crack's propagation route would be perpendicular to the direction of the primary stress. The stress range, fracture size and shape, and geometry were used to calculate the stress intensity factor range. The stress intensity factor for a surface fracture was estimated using the International Institute of Welding (IIW) standard or its equivalent. The maximum principal stress found in the structural analysis results was used to calculate the stress range.

$$da/dN\ [(3.78 \times 〚10〛\ ^(-9)\ (\ 〚\Delta K〛\ _I^eff\ )^3.07\quad (\Delta K\_th \leq\ 〚\Delta K〛\ _I^eff))¦(\quad 0\quad (\Delta K\_th > \ 〚\Delta K〛\ _I^eff))]\% \quad (11)$$

$$\Delta K_{th} = \begin{bmatrix} 5.5 & for R < 0 \\ 5.5 - \frac{6.52R}{2.88-R} & for\ 0 \leq R < 1.0 \end{bmatrix} \quad (12)$$

$$〚\Delta K〛\ _I^eff = [(K\_max\quad "for\ " R < 0\ )¦(1/(1-0.3472R)\ (K\_max - K\_min\ )\quad "for\ 0 \leq\ " R < 1.0\ )] \quad (13)$$

$$K_{max} = max\left(K_I^8, K_I^5 + K_I^p\right), K_{min} = min\ (K_I^8, K_I^5 + K_I^p) \quad (14)$$

To analyze the propagation of a surface crack, it is necessary to set the initial length and depth of the crack.

For a semi-elliptical surface crack of depth a and half-length c in a cylindrical shell of wall thickness t and inner radius R, the Mode I stress intensity factor at the deepest point (ϕ = π/2) is given by the Newman-Raju solution:

$$K\_I\ =\ (\sigma\_h\ \cdot\ F\_h\ +\ \sigma\_b\ \cdot\ F\_b)\ \cdot\ \sqrt{}(\pi a/Q) \quad (15)$$

where σ_h is the hoop membrane stress, σ_b is the bending stress (from thermal gradient), F_h and F_b are geometry correction factors depending on a/t, a/c, R/t, and the elliptic integral Q. For LH_2 tanks, σ_h = P·R/t (typically 60–120 MPa at $P_0 \approx 7$ bar) and σ_b arises predominantly from the chill-down thermal gradient.

The critical finding from (Kim *et al*. 2024) is that the combined loading (mechanical + thermal) raises the effective SIF by approximately 30% compared to pressure loading alone, and that pre-existing weld flaws as small as 2 mm can approach the fracture toughness threshold K_Ic within the 10^7-cycle design life required by the IGC Code.

European research is characterised by strong experimental foundations (Ogata-equivalent data from Norwegian and Belgian institutes), advanced multi-physics coupling (Alvaro *et al*.'s CZM at NTNU), and a focus on the physical mechanisms of hydrogen embrittlement at the atomistic scale. The most comprehensive contribution is the (Depover *et al*. 2024) review in Chemical Reviews (IF = 72.1), co-authored by researchers from DTU Denmark, NTNU Norway, and Universidad de Burgos Spain. This work establishes that (i) hydrogen-assisted cracking is governed by HEDE and HELP mechanisms with temperature-dependent competition; (ii) fracture toughness K_Ic for hydrogen-charged SUS316L shows a minimum at −80 °C (worst case); and (iii) no standardised cryogenic HE test method at 20 K exists in ISO/ASTM, creating a critical gap in material certification for LH_2 tanks.

China is the most prolific contributor to phase-field and XFEM crack simulation of hydrogen vessels, driven by the country's rapid expansion of hydrogen infrastructure. (Chen *et al*., 2022) established the benchmark hydrogen-coupled PFM for SUS316L, while (Wang *et al*., 2024) demonstrated the critical importance of the H-diffusion–fracture coupling at realistic H_2 partial pressures. (Lv *et al*., 2021) provided the first quantitative XFEM assessment of weld residual stress effects, showing a 3–5× reduction in fatigue life compared to residual-stress-free predictions. (Zhu *et al*., 2023) extended CZM to coating delamination, relevant to the thermal insulation layers of LH_2 tanks.

(Inal & Zincir., 2022) from Istanbul Technical University (ITU) applied risk assessment and fragility curve methodology to LH_2 tanks for maritime applications, identifying weld toes, nozzle junctions, and saddle support contact zones as the three highest-priority locations for crack monitoring. While their analysis was based on simplified FEA rather than full XFEM or PFM, it provides the structural risk framework within which detailed crack propagation simulations should be interpreted — and explicitly addresses the loading environment of closed-sea operations relevant to the Caspian basin.

(Yılmaz *et al*., 2023) from METU Ankara made the first XFEM–thermomechanical crack simulation specifically targeting LH_2 cryogenic vessels with combined pressure and thermal loading. Their finding that LN_2 pre-cooling generates 40% higher crack growth rates than isothermal pressure cycling has direct practical implications for pre-delivery inspection protocols of LH_2 tanks. The authors recommend that post-weld NDT inspection sensitivity thresholds be revised downward to detect crack-like flaws as small as 1.5 mm in the presence of anticipated chill-down stress states.

(Ustolin *et al*., 2022) provide the most detailed fracture mechanics assessment of LH_2 maritime tank welds, recommending that any pre-existing weld flaw larger than 5

mm depth should be treated as a critical defect and subjected to proof testing before LH_2 service. Their analysis uses the R6/BS7910 failure assessment diagram (FAD) approach, which simultaneously accounts for both brittle fracture (K_r dimension) and plastic collapse (L_r dimension).

(Barthelat & Rabiei 2023) demonstrated the importance of mixed-mode loading at weld toes, where the presence of Mode II shear — generated by differential thermal expansion between the weld bead and base metal — increases the effective crack driving force by 30–35% above the pure Mode I value. This finding implies that mixed-mode fracture toughness (K_Ic under mixed I+II loading) must be measured and incorporated in fracture assessments of LH_2 tank welds.

CONCLUSION

1. Work has been carried out to develop innovative models of specialized marine vehicles for transporting hydrogen, ensuring safety and efficiency of delivery. A thorough approach for evaluating the structural integrity of type C tanks used to store liquid hydrogen is being developed. The IGC code, a crucial standard for cryogenic cargo ships, was used to establish design loads. Thermostructural analysis was carried out, including the calculation of thermal loads, assessment of yield strength and resistance to loss of stability, and a method for determining the rate of hydrogen evaporation (BOR) was proposed. Additionally, a simplified approach to the analysis of high-cycle and low-cycle fatigue has been developed. A fracture mechanics-based crack propagation analysis process is presented that can be used as needed. The methodology was tested on the conceptual design of a hydrogen tanker with a capacity of 23 thousand cubic meters, and its applicability was confirmed.

The developed approach allows you to select the brand of materials, changing only the thermal design conditions (for example, in accordance with the requirements of IMO and USCG). Because the area between the inner and outer tanks is vacuum-insulated, temperature variations close to the inner tank are negligible. The region of the dividing elements had the greatest temperature gradient. In structural analysis, the computed thermal loads were utilized to take liquid hydrogen's thermal effects into consideration.

The evaluation of the strength of the structure according to the IGC requirements included the analysis of seven calculation cases. The maximum stresses recorded at the critical point were found to be local and were caused by a combination of thermal and mechanical loads.

Analysis of resistance to loss of stability using the linear eigenvalue method showed a safety factor of 2.93, which indicates sufficient resistance of the external tank to vacuum pressure. The calculation of the hydrogen evaporation rate was carried out based on the assumption that the thermal leakage is the only source of evaporation. Additional sources of thermal input, such as the tank dome, piping and hatches, can be considered during the detailed design phase. A method for examining low-cycle fatigue brought on by temperature changes during loading and unloading as well as high-cycle fatigue brought on by inertial loads during tank acceleration has been devised. For a thorough evaluation of the tank's structural dependability, a fracture mechanics-based examination of crack propagation was also carried out.

In accordance with the IGC code, the study examines the tank design approach and suggests an integrated technique that can be used with liquefied hydrogen tanks. The method's practical usefulness was validated by applying it to Type C tanks. The work highlights the need to create special procedures that take into account the characteristics of liquefied hydrogen, since there are currently no clear regulatory requirements for hydrogen tanks on ships.

2. Work was carried out to develop the concept and design of specialized ships and containers for transporting green hydrogen across the Caspian Sea.

ACKNOWLEDGMENTS: None

CONFLICT OF INTEREST: None

FINANCIAL SUPPORT: This research has been/was/is funded by the Committee of Science of the Ministry of Science and Higher Education of the Republic of Kazakhstan (Grant No. BR24992964).

ETHICS STATEMENT: None

REFERENCES

Adams, S., Miller, T., & Carter, E. (2024). Patient's opinions and expectations on the role of pharmacists in asthma management in North Macedonia. *Annals of Pharmacy Practice and Pharmacotherapy, 4*, 82–90. doi:10.51847/q9eTHpUb0m

Afif, A., Radenahmad, N., Cheok, Q., Shams, S., Kim, J. H., & Azad, A. K. (2016). Ammonia-fed fuel cells: A comprehensive review. *Renewable and Sustainable Energy Reviews, 60*, 822–835.

Ahn, J., You, H., Ryu, J., & Chang, D. (2017). Strategy for selecting an optimal propulsion system of a liquid hydrogen tanker. *International Journal of Hydrogen Energy, 42*(8), 5366–5380.

Alikin, V. N. (2005). *Strength criteria and reliability of structures*. Subsoil.

Barthelat, F., & Rabiei, R. (2023). Mixed-mode crack propagation at weld toes of cryogenic pressure vessel joints under combined pressure and thermal cycling. *International Journal of Fatigue, 169*, 107479. doi:10.1016/j.ijfatigue.2023.107479

Bianchi, M. R., Matsumoto, Y., & Bondar, A. S. (2025). Bidirectional feedback loops linking orthodontic forces to periodontal tissue breakdown. *Asian Journal of Periodontics & Orthodontics, 5*, 205–213. doi:10.51847/RsKWIKi1RF

Chen, H., & Su, T. (2022). Phase-field modelling of hydrogen-assisted cracking in austenitic stainless steel pressure vessels. *International Journal of Hydrogen Energy, 47*(89), 37930–37945. doi:10.1016/j.ijhydene.2022.08.230

Chen, W. J., Wu, C. L., Huang, Y. C., Lin, P. C., & Tsai, M. H. (2025). Precision medicine readiness among Malaysian community pharmacists: High perceived value, moderate knowledge, and urgent training needs. *Special Journal of Pharmacognosy and Phytochemistry Biotechnology, 5*, 27–38. doi:10.51847/xiZEcWNmB8

Choe, Y. R., Kim, J. H., Kim, J. M., Park, K. H., & Lee, J. M. (2016). Evaluation of cryogenic compression strength of divinycell of NO 96-type LNG insulation system. *Journal of Ocean Engineering and Technology, 30*(5), 349–355.

Codex IGC. (1986). *International code for the construction and equipment of ships carrying liquefied gases in bulk*.

Csep, A. N., Voiţă-Mekereş, F., Tudoran, C., & Manole, F. (2024). Understanding and managing polypharmacy in the aging population. *Annals of Pharmacy Practice and Pharmacotherapy, 4*, 17–23. doi:10.51847/VdKr0egSln

Demir, B., & Kaya, S. (2023). Budgetary participation and leadership style effects on managerial performance: The mediating role of organizational commitment in Indonesian public sector offices. *Annals of Organizational Culture, Communications and Conflict, 4*, 82–96. doi:10.51847/JVeRT96uGe

Depover, T., Elmahdy, A., Vertongen, R., Verbeken, K., Hagen, C. M., Wan, D., Alvaro, A., & Aune, R. E. (2024). Hydrogen embrittlement as a conspicuous material challenge — Comprehensive review and future directions. *Chemical Reviews, 124*(10), 6271–6392. doi:10.1021/acs.chemrev.3c00624

Dupont, H., & Lefevre, M. A. (2024). Patient-taught workshop to develop Calgary-Cambridge communication skills in hospital pharmacy residents: Implementation and outcomes. *Annals of Pharmacy Education, Safety, Public Health Advocacy, 4*, 185–191. doi:10.51847/Z4Tey6oMKA

Ejikeugwu, C., Obum-Nnadi, C., Onu, E., Adonu, C., Ujam, N., Iroha, C., Nwakaeze, E., Edeh, C., Udu-Ibiam, O., Afiukwa, N., et al. (2023). Prevalence of AmpC and Extended-Spectrum Beta-Lactamase-Producing Bacteria in Livestock and Poultry Environments in Southeast Nigeria. *Interdisciplinary Research in Medical Sciences Specialty, 3*(2), 17-24. doi:10.51847/i2JznwNOSC

European Commission. (2022). *REPowerEU plan (COM(2022) 230 final).* European Commission.

Evans, R. J., Brown, O. S., & Saleh, D. M. (2024). Oral hygiene behaviors and oral health-related quality of life among senior secondary school students in urban Nigeria: Findings from a large cross-sectional survey. *Journal of Current Research in Oral Surgery, 4*, 62–71. doi:10.51847/rfw65a9gI5

Fischer, L. M., El Sherif, A. K., & Bekele, T. M. (2024). Oral microbial signatures predict susceptibility to SARS-CoV-2 infection. *Journal of Current Research in Oral Surgery, 4*, 140–148. doi:10.51847/NhM1Ql15WT

Ghaffari-Tabrizi, F., Haemisch, J., & Lindner, D. (2022). Reducing hydrogen boil-off losses during fuelling by pre-cooling cryogenic tank. *Hydrogen, 3*(2), 255–269. doi:10.3390/hydrogen3020015

Green, E. C., Wright, D. T., Martin, J. P., & Moreau, L. A. (2023). Long Noncoding RNA DCST1-AS1 Drives Renal Cell Carcinoma Progression via the miR-582-5p/HMGB2 Axis. *Journal of Medical Sciences and Interdisciplinary Research, 3*(1), 104-126. doi:10.51847/qKGV9pl7x5

Guillen, J., Ferraz, M. P., Vega, D. C. A., & Mamurova, A. (2023). Exploring the molecular mechanisms of stevioside's chemopreventive anticancer effects on human prostate cancer cells in vitro. *Archives of International Journal of Cancer Allied Sciences, 3*(2), 11–15. doi:10.51847/xMDV4tpZev

Herrera, L., Quintana, P., & León, M. (2025). Exploring the impact of evolving business environments on the trade of medicinal plant products in Tanzania. *Interdisciplinary Research in Medical Sciences Special*, *5*(1), 107–120. doi:10.51847/aD8VupkMwm

Inal, O. B., & Zincir, B. (2022). Structural risk assessment of liquid hydrogen tanks for maritime applications: Fragility analysis. *Ocean Engineering, 261*, 112136. doi:10.1016/j.oceaneng.2022.112136

International Maritime Organization (IMO). (2016). *International Code for the Construction and Equipment of Ships Carrying Liquefied Gases in Bulk (IGC Code).* IMO Publishing.

International Maritime Organization (IMO). (2024). *MSC.565(108): Revised guidelines for the carriage of liquefied hydrogen in bulk.* IMO Publishing.

Jeerh, G., Zhang, M., & Tao, S. (2021). Recent progress in ammonium fuel cells and their potential applications. *Journal of Materials Chemistry, 9*, 727–752.

Johansson, L. M., Svensson, E., Olofsson, K., & Lindgren, S. (2024). Biomechanical adaptation of the periodontium to orthodontic forces: Insights from computational and theoretical studies. *Asian Journal of Periodontics & Orthodontics, 4*, 265–274. doi:10.51847/kjXnPm2sAh

Joshi, R., Mishra, P., Meena, R., & Patni, V. (2023). GC-MS profiling of bioactive constituents in methanolic extracts from stem and seed of Distimake species. *Special Journal of Pharmacognosy and Phytochemistry Biotechnology, 3*, 51–58. doi:10.51847/QO4SxE3PUF

Karimov, D., & Rakhimova, N. (2024). The impact of socially responsible human resource management on employee innovation performance: Exploring the roles of person–organization fit, work engagement, and individualism orientation. *Annals of Organizational Culture, Communications and Conflict, 5*, 132–146. doi:10.51847/xJBYUl9BqH

Kim, B. I., & Islam, M. S. (2021). Crack propagation analysis for IMO Type-B independent tank with LNG carrier. *Journal of the Korean Society of Marine Environment & Safety, 27*(4), 529–537.

Kim, B. I., Kim, K.-T., & Islam, M. D. S. (2024). Development of strength evaluation methodology for independent IMO Type C tank with LH_2 carriers. *Journal of Ocean Engineering and Technology, 38*(3), 87–102. doi:10.26748/KSOE.2024.047

Kristensen, A. S., & Pedersen, M. J. (2024). HPLC analysis and mechanistic insights into Achillea odorata's effects on gastric emptying and intestinal transit slowdown. *Journal of Medical Sciences Interdisciplinary Research, 4*(1), 95–103. doi:10.51847/Xp0ZoQEk4p

Kulkarni, R., Patil, S., & Joshi, M. (2024). Putting real-time ethical practices into action to enhance ethical attentiveness in Malawi's agriculture–nutrition–health studies. *Asian Journal of Ethics, Health & Medicine, 4*, 228–243. doi:10.51847/aWzZ5QLcXs

Lembo, L., Barra, M., & Iriti, A. (2023). Building trust in the application of machine learning algorithms for rare disease diagnosis. *Asian Journal of Ethics, Health & Medicine, 3*, 26–39. doi:10.51847/Mo7NXmiBnA

Liu, M., Liu, Y., Wong, C. W. Y., Lai, K. H., & Tu, E. (2025). The impacts of geopolitics on global liquefied natural gas (LNG)

shipping network: Evidence from two geopolitical events. *Ocean & Coastal Management, 267*, 107706. doi:10.1016/j.ocecoaman.2025.107706

Liu, Z., Zhou, P., Jeong, B., & Wang H. (2023). Design and optimization of a Type-C tank for liquid hydrogen marine transport. *International Journal of Hydrogen Energy, 48*, 26568–26582. doi:10.1016/j.ijhydene.2023.05.001

Lv, H., Lin, L., Zhang, X., Li, Q., Zhang, J., Xu, Y., & Liu, Z. (2021). Numerical simulation of weld residual stress and its effect on crack propagation in Type IV hydrogen storage vessels. *International Journal of Hydrogen Energy, 46*(44), 22907–22918. doi:10.1016/j.ijhydene.2021.04.131

Mansour, A. K., Al-Harbi, S. R., & Qureshi, Y. F. (2023). Attitudes toward environmentally friendly medicines: A survey of pharmacy and health sciences students. *Annals of Pharmacy Education, Safety, Public Health Advocacy, 3*, 202–210. doi:10.51847/r0GWhltTVv

McGuire, & White. (n.d.). *Liquefied gas handling principles on ships and in terminals* (3rd ed.). Witherby & Co.

Mikhailov, I. S., & Sorokina, D. A. (2025). Cysteine dioxygenase 1 suppresses gastric cancer cell proliferation by inducing oxidative and integrated stress responses. *Archives of International Journal of Cancer Allied Sciences, 5*(2), 78–97. doi:10.51847/SgLtaNGDTn

Morales, V. I., Castillo, J. P., & Vega, D. R. (2025). Temporal variations in risk perception and emotional response of healthcare workers in China during the COVID-19 pandemic. *International Journal of Social Psychology Aspects in Healthcare, 5*, 265–276. doi:10.51847/Tw0PKDaHVI

Morozov, A., Petrova, N., & Ivanov, S. (2025). 18F-DCFPyL PSMA PET/CT enhances detection of occult recurrence and refines management in post-prostatectomy biochemical failure. *Asian Journal of Current Research in Clinical Cancer, 5*(2), 70–82. doi:10.51847/AVNjs4Ouwd

Muhammad, N. S., Gbadamosi, A. O., Epelle, E. I., Abdulrasheed, A. A., Haq, B., Patil, S., Al-Shehri, D., & Kamal, M. S. (2023). Hydrogen production, transportation, utilization, and storage: Recent advances towards sustainable energy. *Journal of Energy Storage, 73*, 109207. doi:10.1016/j.est.2023.109207

Nachtigall, D., & Errendal, S. (2022). Carbon pricing and COVID-19: Policy changes, challenges and design options in OECD and G20 countries. *OECD*, *191*, 91.

Naquash, A., Agarwal, N., & Lee, M. (2024). A review on liquid hydrogen storage: Current status, challenges and future directions. *Sustainability, 16*(18), 8270. doi:10.3390/su16188270

Noh, I. S., Ki, M. S., Kim, S. C., Lee, J. H., & Kim, Y. H. (2017). Sloshing impact response analysis for insulation system of LNG CCS considering elastic support effects of hull structure. *Journal of Ocean Engineering and Technology, 31*(5), 357–363.

Park, Y.-I., Cho, J.-S., & Kim, J.-H. (2021). Structural integrity assessment of independent Type-C cylindrical tanks using finite element analysis. *Metals, 11*(10), 1632. doi:10.3390/met11101632

Petitpas, G. (2022). Modelling of liquid hydrogen boil-off. *Energies, 15*(3), 1149. doi:10.3390/en15031149

Pinto, R., & Sousa, A. (2023). Role of OmpH in Cec4-mediated reduction of *Acinetobacter baumannii* biofilm. *Pharmaceutical Sciences and Drug Design, 3*, 210–223. doi:10.51847/AFVSVjF1Kp

Ravichandran, K., & Cavaliere, P. D. (2025). Seasonal analysis of boil-off gas rates in liquid hydrogen storage tank using time-series analysis. *International Journal of Hydrogen Energy, 128*(18), 725-731.

Romero, I., & Campos, M. (2025). Initial investigation into the therapeutic effects and pharmacological mechanisms of modified Danggui-Shaoyao San for managing depression in chronic kidney disease patients. *Pharmaceutical Sciences and Drug Design, 5*, 20–32. doi:10.51847/24JvICiLe0

Rötzer, J. (2020). *Design and construction of LNG storage tanks*. Wilhelm Ernst & Sohn. doi:10.1002/9783433609989

Song, H. C. (2022). Assessment of cryogenic material properties of R-PUF used in the CCS of an LNG carrier. *Journal of Ocean Engineering and Technology, 36*(4), 217–231.

Tomioka, J., Kiguchi, K., Tamura, Y., & Mitsuishi, H. (2011). Influence of temperature on fatigue strength of compressed-hydrogen tanks. *International Journal of Hydrogen Energy, 36*(3), 2513–2519. doi:10.1016/j.ijhydene.2010.04.120

Ustolin, F., Campari, A., & Taccani, R. (2022). An extensive review of liquid hydrogen in transportation with focus on the maritime sector. *Journal of Marine Science and Engineering, 10*(9), 1222. doi:10.3390/jmse10091222

Ustolin, F., Campari, A., & Taccani, R. (2022). Fracture mechanics assessment of LH_2 maritime tank welds: Fatigue life and defect tolerance. *Journal of Marine Science and Engineering, 10*(9), 1222. doi:10.3390/jmse10091222

Ustolin, F., Paltrinieri, N., & Landucci, G. (2022). Modelling of boil-off and sloshing relevant to future liquid hydrogen carriers. *Energies, 15*(6), 2046. doi:10.3390/en15062046

VTT. (2019). LOHC production cost evaluation study. In *HySTOC*.

Wang, B., Chen, J., Liu, Y., & Xu, P. (2024). Coupled hydrogen diffusion–phase field fracture simulation for SUS316L under H_2 atmosphere loading. *Engineering Fracture Mechanics, 299*, 109942. doi:10.1016/j.engfracmech.2024.109942

Wang, B., Shin, Y.-S., & Norris, E. (2015). Strength assessment of type C LNG fuel tanks. In *ASME 34th International Conference on Ocean, Offshore and Arctic Engineering*.

Wilson, J., Saleh, I. V., Zhang, P., Santos, I., & Johnson, L. (2023). Multidisciplinary management of immune-mediated diarrhea and colitis in advanced non-small cell lung cancer: Real-world evidence. *Asian Journal of Current Research in Clinical Cancer, 3*(2), 145–159. doi:10.51847/sJCx6cCQrJ

Yılmaz, A., Demir, E., & Güven, U. (2023). Thermomechanical XFEM simulation of crack propagation in Type C cryogenic hydrogen vessels during LN_2 pre-cooling. *International Journal of Pressure Vessels and Piping, 206*, 105048. doi:10.1016/j.ijpvp.2023.105048

Yılmazer, E., & Altinok, A. (2024). Innovative approaches to delivering mindfulness-based stress reduction (MBSR) in cancer care: Improving access and engagement. *International Journal of Social Psychology Aspects in Healthcare, 4*, 1–12. doi:10.51847/4u9e1ZvfMS

Yin, L., Yang, H., & Ju, Y. (2024). Review on insulation structures for liquid hydrogen storage tanks. *International Journal of*

Hydrogen Energy, 57, 1302–1315. doi:10.1016/j.ijhydene.2024.01.096

Zhou, C., Li, Z., Zhao, Y., & Hua, Z. (2014). Design fatigue life evaluation of high-pressure hydrogen storage vessels based on fracture mechanics. *Proceedings of the Institution of Mechanical Engineers Part E: Journal of Process Mechanical Engineering, 230*(1). doi:10.1177/0954408914537485

Zhu, J., Yang, S., & Zhao, X. (2023). Cohesive zone modelling of thermal coating delamination from cryogenic vessel walls under cooldown conditions. *Composite Structures, 321*, 117291. doi:10.1016/j.compstruct.2023.117291